Inorganic Chemistry

Article

pubs.acs.org/IC

Microporous Metal–Organic Framework Based on a Bifunctional Linker for Selective Sorption of CO_2 over N_2 and CH_4

Di-Ming Chen, Xiao-Ping Zhang, Wei Shi,* and Peng Cheng*

Department of Chemistry, Key Laboratory of Advanced Energy Materials Chemistry (MOE), and Collaborative Innovation Center of Chemical Science and Engineering (Tianjin), Nankai University, No. 94, Weijin Road, Tianjin 300071, P. R. China

Supporting Information

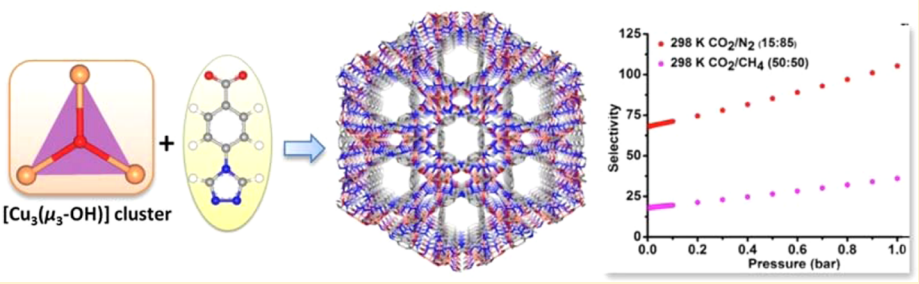

ABSTRACT: A bifunctional organic linker 4-(4-carboxyphenyl)-1,2,4-triazole (HCPT), incorporating both carboxylate and triazole groups, has been successfully used in the construction of a 2-fold interpenetrated dynamic metal–organic framework (MOF), $\{[Cu_3(CPT)_4(\mu_3\text{-}OH)]\cdot NO_3\cdot 7H_2O\cdot EtOH\}_n$ (**1**) based on a triangular Cu(II)-hydroxo cluster as secondary building unit (SBU). Upon solvation/desolvation and temperature, the crystal cell parameters of **1** could be fine-tuned. More importantly, a transformation from disordered phase to a more ordered phase after activation was observed via a single-crystal-to-single-crystal mode. Gas sorption studies reveal that the activated **1** exhibits highly selective sorption of CO_2 over N_2 and CH_4 at room temperature.

INTRODUCTION

Over the past decade, a new family of crystalline porous material named metal–organic frameworks (MOFs) has attracted much attention by scientific community for its large surface areas, designable frameworks, adjustable pore surface functionality, and tunable pore sizes and shapes.[1−3] This kind of advanced material has already shown great potential for many applications such as CO_2 capture and separation (CCS).[4−7] With the rapid development of industry, a great amount of CO_2 has been released into the atmosphere, which is now known to cause severe global warming and climate changes.[8] The purification of low-quality natural gas by removing CO_2 from it has also become an important issue. Hence, the CCS process has become a subject of widespread concern, in both industrial and environmental aspects. As an emerging class of porous crystalline materials, MOFs have recently been explored as a potential new class of CO_2 adsorbents.[9−15] Up to now, only few MOFs exhibit highly selective sorption of CO_2 over both of N_2 and CH_4.[16] The rational design and synthesis of MOFs with high CO_2 capture and selectivity still remains a great challenge for chemists, especially at ambient temperature and pressure, because the CO_2 adsorption capacity and selectivity are affected by many factors such as the electronic environment of the framework, pore size, surface areas, and so on.[17−20]

In the exploration of MOFs for effective CO_2 separation, researchers have developed several strategies such as functional group gifting, pore-size control, open metal sites (OMS), and postmodification.[21] In general, MOFs are composed of metal ions or in situ generated clusters as nodes and organic ligands as linkers, so the deliberate selection of the nodes and linkers is the key factor for desirable structures and properties. Organic linkers incorporating carboxylate or triazole groups are two kinds of the most widely used ligands in MOF chemistry which have been demonstrated to be excellent to construct MOFs for their diverse coordination models and strong binding abilities.[22,23] To combine the merits of both the carboxylate and triazole groups, the bifunctional ligand 4-(4-carboxyphenyl)-1,2,4-triazole (HCPT) was selected as the organic linker. We previously prepared a cage-based cationic MOF with $[Cu_4Cl]^{7+}$ cluster as the node under solvothermal conditions. However, it was not robust enough to explore the CO_2 storage property.[24] In this work, a new 2-fold interpenetrated MOF $\{[Cu_3(CPT)_4(\mu_3\text{-}OH)]\cdot NO_3\cdot 7H_2O\cdot EtOH\}_n$ (**1**) containing a triangular Cu(II)-hydroxo cluster as secondary building unit (SBU) was synthesized under hydrothermal conditions (Scheme 1). This MOF not only shows structural changes upon external stimuli, but also displays highly selective sorption of CO_2 over N_2 and CH_4 at room temperature.

Received: March 11, 2015
Published: May 19, 2015

DOI: 10.1021/acs.inorgchem.5b00561
Inorg. Chem. 2015, 54, 5512−5518

Scheme 1. Synthetic Route for 1 with Photo of the Hexagonal Crystals of 1

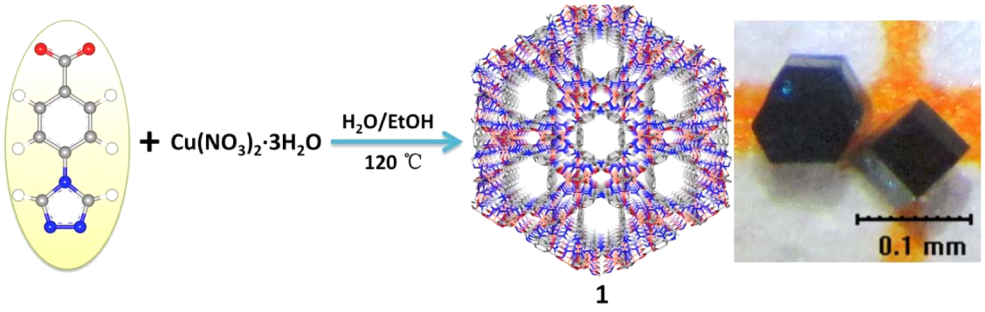

Scheme 2. Synthetic Routes for 1a, 1b, and 1c

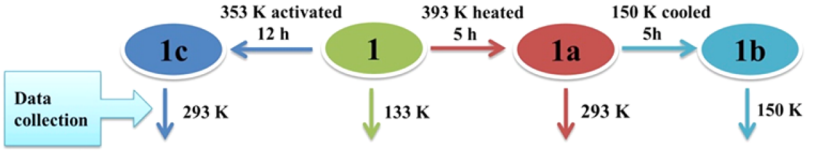

1c (C_2/c)	1 (C_2/c)	1a (P_2/c)	1b (P_2/c)
a = 25.7877(6) Å b = 14.8425(4) Å c = 26.8476(12) Å	a = 25.4902(4) Å b = 14.7273(2) Å c = 27.1139(5) Å	a = 25.6014(3) Å b = 14.8269(2) Å c = 26.8476(12) Å	a = 25.5831(5) Å b = 14.8084(3) Å c = 27.2527(11) Å
β = 91.062(3) °	β = 94.659(2) °	β = 94.322(1) °	β = 94.656(3) °

Table 1. Crystallographic Data and Structure Refinement Details for 1

	1	1a	1b	1c
formula	$C_{38}H_{45}Cu_3N_{13}O_{20}$	$C_{72}H_{48}Cu_6N_{26}O_{24}$	$C_{72}H_{48}Cu_6N_{26}O_{24}$	$C_{36}H_{24}Cu_3N_{13}O_{12}$
fw	1194.49	2042.66	2042.66	1021.33
T (K)	133(3)	293(2)	150.05(10)	293(2)
cryst syst	monoclinic	monoclinic	monoclinic	monoclinic
space group	C_2/c	P_2/c	P_2/c	C_2/c
a (Å)	25.4902(4)	25.6014(3)	25.5831(5)	25.7877(6)
b (Å)	14.7273(2)	14.8269(2)	14.8084(3)	14.8425(4)
c (Å)	27.1139(5)	27.3104(4)	27.2527(11)	26.8476(12)
α (deg)	90.00	90.00	90.00	90.00
β (deg)	94.659(2)	94.322(1)	94.656(3)	91.062(3)
γ (deg)	90.00	90.00	90.00	90.00
V (Å^3)	10 145.0(3)	10 337.3(2)	10 290.5(5)	10 274.3(6)
Z	8	4	4	8
D_c (g/cm^3)	1.564	1.313	1.318	1.322
μ (mm^{-1})	1.333	1.286	1.292	1.294
R_{int}	0.0297	0.0246	0.0402	0.0417
collected/unique	41 077/8971	37 943/18 202	38 885/18 114	19 046/9039
GOF on F^2	1.060	1.104	1.094	1.026
R1, wR2 [$I > 2\sigma(I)$]	0.0576/0.1587	0.0546, 0.1601	0.0683, 0.1936	0.0494, 0.1318
R1, wR2 (all data)	0.0612/0.1626	0.0665, 0.1677	0.0919, 0.2072	0.0616, 0.1404
largest peak and hole (e Å^{-3})	2.23/−1.23	2.46/−0.75	3.63/−0.95	1.47/−0.59
CCDC number	1034262	1034263	1034264	1034265

EXPERIMENTAL SECTION

Materials and Methods. Ligand 4-(4-carboxyphenyl)-1,2,4-triazole (HCPT) was prepared according to the modified literature procedure,[25] and other reagents are commercially available and used without further purification. FT-IR spectra were measured with a Bruker Tensor 27 Spectrometer on KBr discs in the 4000−400 cm^{-1} region. Elemental analyses for C, H, and N were carried out by a PerkinElmer analyzer. Thermal analyses (under N_2 atmosphere, heating rate of 10 °C min^{-1}) were carried out in a Labsys NETZSCH TG 209 Setaram apparatus from room temperature to 800 °C. Powder X-ray diffraction measurements were measured using a D/Max-2500 X-ray diffractometer with Cu Kα radiation. N_2, CO_2, and CH_4 sorption isotherms were recorded on the gas adsorption analyzer Autosorb-IQ2 (Quantachrome Instruments).

DOI: 10.1021/acs.inorgchem.5b00561
Inorg. Chem. 2015, 54, 5512−5518

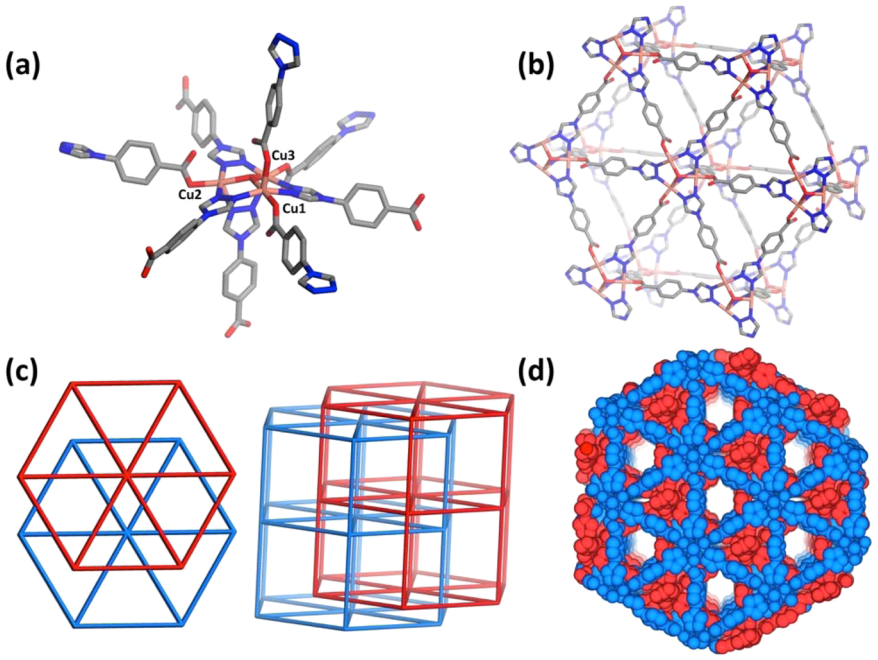

Figure 1. (a) Trinuclear copper SBU in the framework of **1**. (b) The 3^6 net pillared by CPT ligands along *c* axes. (c) The 2-fold interpenetrated hex net. (d) The space filling model of the framework.

Synthesis of $\{[Cu_3(CPT)_4(\mu_3\text{-}OH)]\cdot NO_3\cdot 7H_2O\cdot EtOH\}_n$ (1). A mixture of $Cu(NO_3)_2\cdot 3H_2O$ (0.048 g, 0.2 mmol), HCPT (0.020 g, 0.1 mmol), H_2O (4 mL), and EtOH (2 mL) was added to a 25 mL Teflon-lined stainless steel reactor, and then heated at 120 °C for 2 days under autogenous pressure. After being cooled to room temperature, blue block crystals were obtained by filtration, washed with H_2O and EtOH in sequence, and dried in air. The yield was 78% (based on HCPT). IR (KBr, cm^{-1}): 3420 (br), 3014 (br), 2094 (w), 1606 (s), 1541(s), 1390 (s), 1254 (s), 1016 (s), 847 (m), 783 (s), 698 (m). Anal. Calcd (%) for **1** ($C_{38}H_{45}Cu_3N_{13}O_{20}$): C, 38.21; H, 3.80; N, 15.24. Found: C 38.36 H 3.89, N 15.08. A single crystal of **1a** was obtained by heating a well-diffracted single crystal of **1** on an Oxford Supernova TM diffractometer equipped with temperature controller at 393 K for 5 h, and **1b** was afforded by cooling **1a** at 150 K for 5 h; **1c** was obtained by outgassing a well-diffracted single crystal of **1** under vacuum at 80 °C for 12 h on the gas adsorption analyzer (Scheme 2).

X-ray Crystallography. Data collections for **1**−**1c** were performed on an Oxford Supernova TM diffractometer with graphite-monochromated Mo Kα radiation (λ = 0.710 73 Å) using ω-scan technique. The SHELXL-97 program was used to solve and refine the targeted structures based on direct method and full matrix least-squares technique.[26] Anisotropic thermal parameters were assigned to all non-hydrogen atoms. The hydrogen atoms of organic ligand were generated geometrically. For all structures the contribution of heavily disordered solvent molecules was treated by the Squeeze procedure implemented in Platon.[27] For **1**−**1b**, DFIX, SADI, DELU, and ISOR commands were used in the refinement of the two positional disorder CPT ligands. For **1c**, the ISOR common was used in the refinement of the NPD atom C32. Details for structural analysis are summarized in Table 1.

RESULTS AND DISCUSSION

Synthesis and Structure. Hydrothermal reaction of $Cu(NO_3)_2\cdot 3H_2O$ and HCPT in H_2O/EtOH (2:1, v/v) at 120 °C for 48 h resulted in dark blue hexagonal crystals of **1** with high yield (Scheme 1, Supporting Information Figure S1). Single-crystal X-ray study reveals that **1** crystallizes in monoclinic space group C_2/c and possesses a 2-fold interpenetrated 3D framework. There is one $[Cu_3(\mu_3\text{-}OH)]^{5+}$ cluster with three crystallographically independent Cu(II) atoms in one asymmetric unit; all Cu(II) atoms exhibit pentacoordinate square-pyramidal environments (Figure 1a). Cu1 is connected with two nitrogen atoms and two carboxylic oxygen atoms from four individual CPT ligands, and one oxygen atom from the μ_3-OH. Cu2 is bonded with three nitrogen atoms and one carboxylic oxygen atom from four individual CPT ligands, and one oxygen atom from the μ_3-OH. Cu3 adopts the same connection mode as Cu2. Three Cu(II) ions along with three triazole units form a trinuclear SBU in which the Cu(II) ions are additionally bridged by μ_3-OH. The NO_3^- ions are housed in the interlayer of the framework, so they do not occupy the channel space (Supporting Information Figure S2). When it is viewed along the *ab* plane, each $[Cu_3(\mu_3\text{-}OH)]^{5+}$ cluster is connected to six adjacent ones via CPT to form a triangle-tessellated layer structure with trigonal windows (Figure 1b). With the consideration of the trinuclear motifs as 6-connected nodes and the ligands as 2-connected linkers, the layer can be considered as a 3^6 net. These layers are further pillared by CPT along *c* axes to afford a 8-connected 3D frameworks 2-fold interpenetrated with a point symbol $\{3^6.4^{18}.5^3.6\}$ that belongs to hexagonal primitive (hex) topology (Figures 1c and 2). To the best of our knowledge, the pillared 2D 3^6 layer in MOFs based on single-ligand is rarely reported, and **1** represents the first example of MOFs showing hex topology based on a triazolcarboxylate ligand.[28] It is interesting to notice that the topology of **1** resembles its crystal shape. In the framework, there are one-dimensional channels with a diameter *ca.* 6.02 Å running along the [001] direction calculated by *Poreblazer* software (Figure 1d).[29] The solvent-accessible volume was calculated (PLATON program) to be 30.6% of the crystal volume.[30]

Powder X-ray Diffraction (PXRD), Thermal Gravimetric Analyses (TGA), and Framework Flexibility. The powder X-ray diffraction (PXRD) pattern of **1** has been measured at room temperature to evaluate its phase purity. The collected data is consistent with the simulated one from the

DOI: 10.1021/acs.inorgchem.5b00561
Inorg. Chem. 2015, 54, 5512−5518

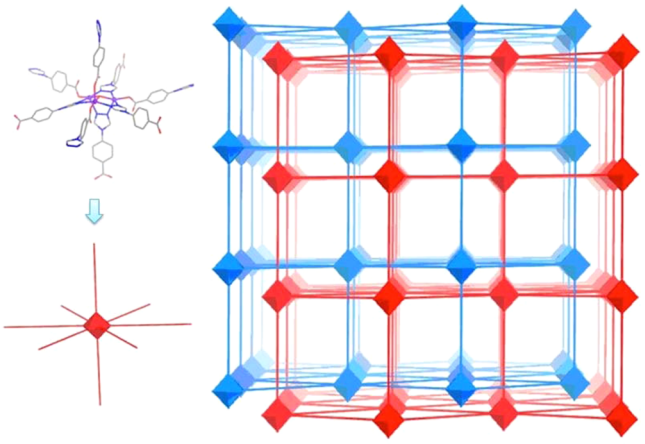

Figure 2. Schematic representation of the topological structure of **1**; the blue net and the red net are interpenetrating with each other.

single-crystal data, indicative of its high phase purity (Figure 4). Thermal stability was evaluated by thermogravimetric analysis (TGA) and variable-temperature PXRD (Supporting Information Figures S4 and S5), and both show that **1** could be stable up to 260 °C. The TGA curve of **1** shows a weight loss of 14.3% in the temperature ranging from 25 to 110 °C, which could be due to the escape of seven lattice H_2O and one EtOH molecules (calcd 14.4%), and then a platform appears up to 260 °C. Recent research reveals that some interpenetrated frameworks show interesting structural changes by external stimuli.[31] To investigate the dynamic structural property of **1**, a well-diffracted single crystal was heated on the X-ray diffractometer at 393 K for 5 h to give **1a** $\{[Cu_3(CPT)_4(\mu_3\text{-}OH)]\cdot NO_3\}_n$ (Scheme 2). The structural determination of **1a** showed that the unit-cell parameters *a*, *b*, and *c* changed +0.44%, +0.68%, and +0.7% compared with those of **1**, respectively. Meanwhile, its β angle also decreased 0.36% with the space group change from C_2/c to P_2/c. After data collection, the single crystal was cooled at 150 K for 5 h to give **1b** with the same formula of **1a**. The unit-cell parameters *a*, *b*, and *c* of **1b** changed +0.07%, −0.12%, −0.2% with the β angle decreased 0.35% compared with that of **1a**. It is noticed that the original crystal parameters cannot be generated by simply returning to the original temperature because of the loss of the lattice molecules. The crystal data of **1c** (obtained by outgassing a well-diffracted single crystal of **1** under vacuum at 80 °C overnight) was also collected for further study, which showed the unit-cell parameters *a*, *b*, and *c* changed +1.2%, +0.8%, −0.98% with β angle decreased 3.8% compared with those of **1**. Although these crystal cell parameters were only fine-tuned, the pore sizes are still sensitive to external stimuli as calculated by *Poreblazer* software. The calculated results revealed the max pore diameter was 6.02, 6.18, 6.00, and 6.32 Å for **1**, **1a**, **1b**, and **1c**, respectively (Figure 3). Since the hexagonal channels are defined by intersection of the trigonal channels from the two identical interpenetrated networks, their pore diameters largely depend on the relative position of each independent framework. The changes of distance between the μ_3-OH of each interpenetrated structure confirm the movement of the network (Supporting Information Figure S6). It is interesting that the two positional disordered CPTs in **1** could not be found in **1c** (Supporting Information Figure S7), revealing a transformation from a disordered phase to a more ordered phase after activation which may result from the stronger interframework interactions. The PXRD patterns of **1c** were right shifted a little compared with that of **1** (Figure 4). However, they could restore to that of **1** after soaking in MeOH for 3 days, indicating the dynamic structure of **1**.[32] Such a type of dynamic behavior is distinguishable from those which possess a large breathing effect along with void volumes and drastic swelling of the cells.[33]

Gas Adsorption Studies. Inspired by its moderate void volume and dynamic structural nature, the gas adsorption property of **1** was studied. Before the measurements, about 100 mg of crystals of **1** was finely treated ultrasonically and soaked in MeOH for 3 days, and then outgassed under dynamic vacuum at 80 °C overnight to afford **1c**. The surface areas were calculated on the basis of the CO_2 isotherm collected at 195 K in a relative pressure ranging from 10^{-3} to 1 atm. It showed a max uptake of 121 cm^3/g with type-I behavior. The surface areas calculated from CO_2 sorption data are 386 m^2/g (BET)

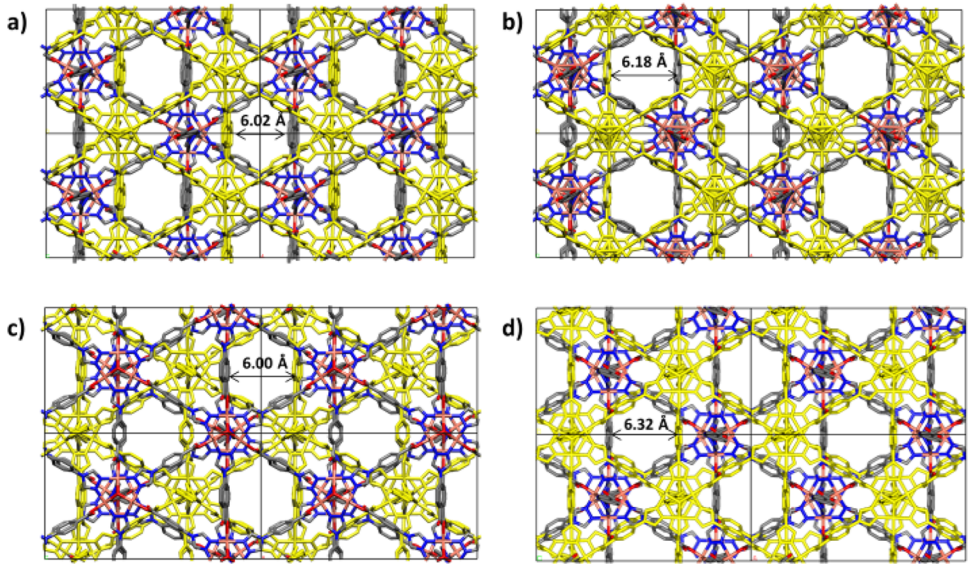

Figure 3. Pore diameters calculated by software *Poreblazer*: (a) orginal data, (b) after being heated, (c) after being cooled, and (d) after activation.

DOI: 10.1021/acs.inorgchem.5b00561
Inorg. Chem. 2015, 54, 5512−5518

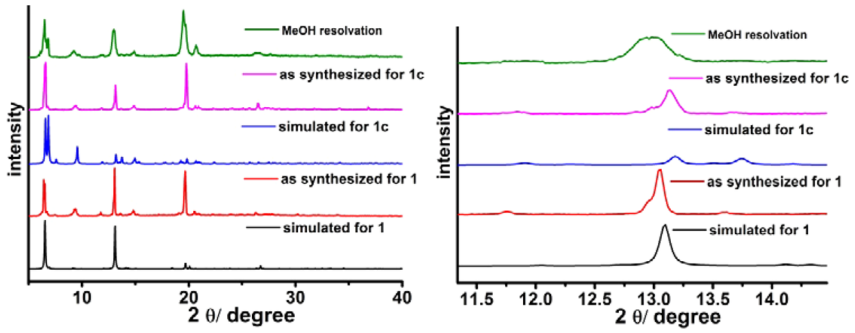

Figure 4. PXRD patterns of **1** and **1c**.

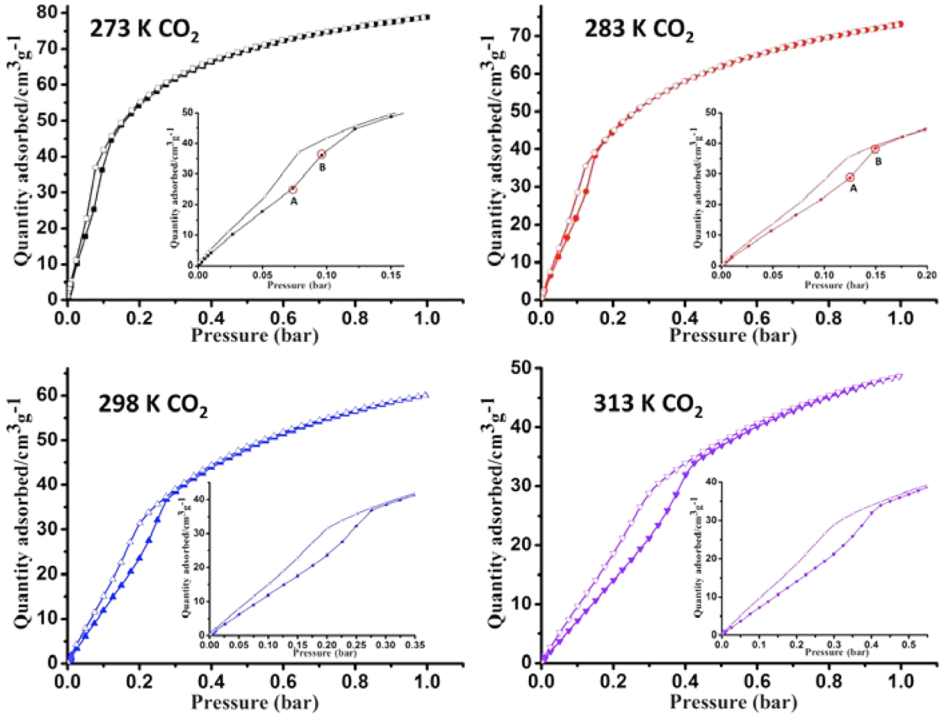

Figure 5. CO_2 isotherms of **1c** at different temperatures.

and 472 m^2/g (Langmuir), respectively. It is very interesting that **1c** showed hysteresis in the desorption of CO_2, which may be explained by strong interaction of the CO_2 molecules with the framework.[34] At 273 K, the isotherm of CO_2 showed an unconspicuous two-step sorption with a slight hysteresis: **1c** can capture 25.3 cm^3/g of CO_2 at 0.074 atm, and then a jump in uptake occurs until the pressure of 0.1 atm with a uptake of 36.2 cm^3/g, and further increased to 78.8 cm^3/g at 1 atm (Figure 5). At 283 K, **1c** showed an uptake of 28.7 cm^3/g of CO_2 at 0.13 atm, and an abrupt increase was observed at the pressure of 0.16 atm, which was followed by a slow increase to the max uptake of 73.1 cm^3/g at 1 atm. Isotherms at 298 and 313 K show similar trends, with the max uptake of 60.1 and 48.7 cm^3/g, respectively. As shown in Figure 4, a few PXRD patterns change upon guest removal/recover suggesting the dynamic framework to some degree. So the present unconspicuous stepwise gas sorption isotherms might be attributed to the guest-induced reversible phase transitions on gas adsorption and desorption, which has been encountered in some 2-fold interpenetrated MOFs with stepwise sorption behavior reported recently.[35,36] The width of the hysteresis loops in the CO_2 adsorption isotherms turn out to be more pronounced as the temperature increases, accompanying the phase transition pressure shifts toward higher pressure. Such behavior is the typical characteristic of porous MOFs with flexible pores which could be triggered by gas molecules.[37−40]

For comparison, N_2 and CH_4 sorption isotherms were measured at 273 and 298 K, and showed type-I character with uptakes of 3.1, 2.5 cm^3/g for N_2 and 13.0, 8.2 cm^3/g for CH_4, respectively (Figure 6). The selectivity of CO_2 over N_2 and CH_4 from a binary gas mixture was evaluated by the ideal adsorbed solution theory (IAST) based on CO_2, CH_4, and N_2 isotherms measured.[41] In general, the IAST selectivity for CO_2/CH_4 and CO_2/N_2 decreases slightly as the pressure increases.[42,43] Interestingly, **1c** shows increasing trend with a high $S_{ads}(CO_2/N_2)$ of 105 in a 15:85 molar ratio of CO_2 and N_2 mixtures at 298 K and 1 atm. The $S_{ads}(CO_2/CH_4)$ at 298 K shows a similar increasing trend from 18 to 36 at 298 K. The $S_{ads}(CO_2/CH_4)$ of **1c** under room temperature is higher than most MOFs under similar conditions.[3] The experimental result suggests that **1c** is a promising candidate for separation of CO_2 from CH_4. To better understand the CO_2−framework interaction, isosteric heats (Q_{st}) of CO_2 were calculated with the virial method on the basis of CO_2 isotherms collected at

DOI: 10.1021/acs.inorgchem.5b00561
Inorg. Chem. 2015, 54, 5512−5518

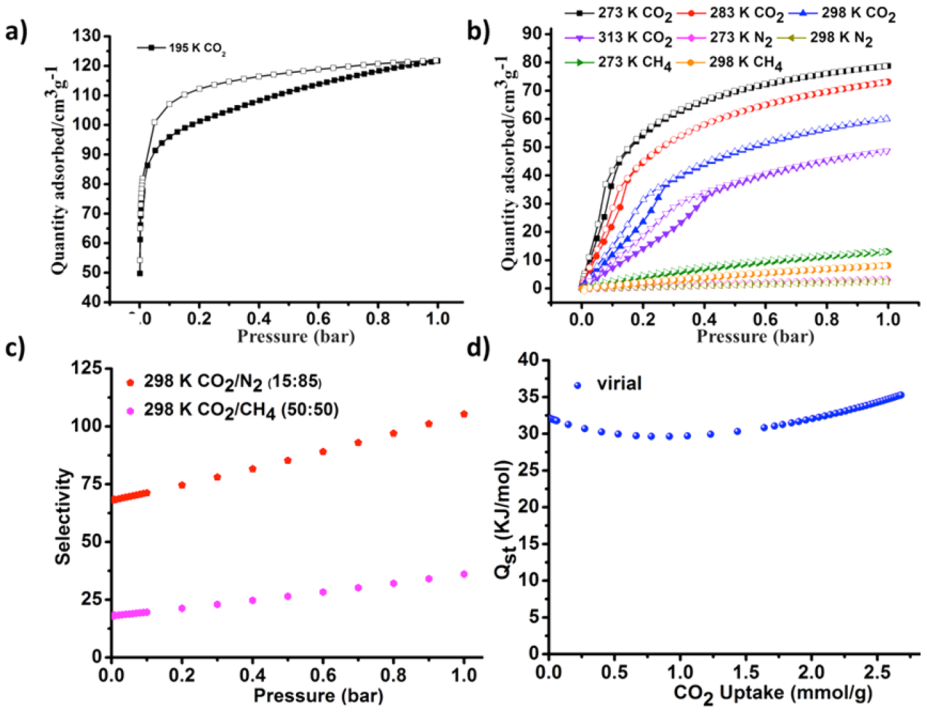

Figure 6. (a) CO_2 sorption isotherm of **1c** at 195 K. (b) CO_2, CH_4, and N_2 sorption isotherms of **1c** around room temperature. (c) IAST predicted CO_2/N_2 and CO_2/CH_4 selectivity at 298 K. (d) CO_2 isosteric adsorption enthalpy calculated from virial method.

273 and 298 K (Supporting Information Figure S8). The Q_{st} is 32 kJ mol^{-1} at zero loading, which indicates strong interaction between the framework and CO_2.[44] After initial loading, the Q_{st} falls slowly and then rises again to a value that is higher than that at zero loading, which might be attributed to the strong interactions between the adsorbed CO_2 molecules.[45,46]

CONCLUSION

In conclusion, a 2-fold interpenetrated dynamic MOF, **1**, has been successfully assembled from the triangular Cu(II)−hydroxo cluster and the bifunctional organic linker HCPT, whose structure responds to external stimuli. MOF **1** shows stepwise and hysteretic CO_2 sorption isotherms and highly selective sorption of CO_2 over N_2 and CH_4 at room temperature, which endows this MOF with promising utilization in CO_2 storage and purification of natural gas. Further studies on the construction of MOFs based on HCPT ligand and other SBUs are under way in our lab.

ASSOCIATED CONTENT

Supporting Information

Additional structural pictures (Figures S1−S3), variable-temperature powder X-ray diffraction patterns (Figures S4), TGA curves (Figure S5), fitting details of sorption isotherms (Figure S6), and X-ray crystallographic information in CIF format for **1**−**1c**. The Supporting Information is available free of charge on the ACS Publications website at DOI: 10.1021/acs.inorgchem.5b00561.

AUTHOR INFORMATION

Corresponding Authors

*E-mail: shiwei@nankai.edu.cn.
*E-mail: pcheng@nankai.edu.cn.

Notes

The authors declare no competing financial interest.

ACKNOWLEDGMENTS

We thank the "973 Program" (2012CB821702), NSFC (21421001), the MOE (IRT-13R30), 111 Project (B12015), the NSF of Tianjin (13JCZDJC32200) for financial support.

REFERENCES

(1) Zhou, H.-C.; Kitagawa, S. *Chem. Soc. Rev.* **2014**, *43*, 5415−5418.
(2) Zhou, H.-C.; Long, J. R.; Yaghi, O. M. *Chem. Rev.* **2012**, *112*, 673−674.
(3) Long, J. R.; Yaghi, O. M. *Chem. Soc. Rev.* **2009**, *38*, 1213−1214.
(4) Sumida, K.; Rogow, D. L.; Mason, J. A.; McDonald, T. M.; Bloch, E. D.; Herm, Z. R.; Bae, T.-H.; Long, J. R. *Chem. Rev.* **2012**, *112*, 724−781.
(5) Li, J.-R.; Sculley, J.; Zhou, H.-C. *Chem. Rev.* **2012**, *112*, 869−932.
(6) Cui, P.; Ma, Y.-G.; Li, H.-H.; Zhao, B.; Li, J.-R.; Cheng, P.; Balbuena, P. B.; Zhou, H.-C. *J. Am. Chem. Soc.* **2012**, *134*, 18892−18895.
(7) Nugent, P.; Belmabkhout, Y.; Burd, S. D.; Cairns, A. J.; Luebke, R.; Forrest, K.; Pham, T.; Ma, S.; Space, B.; Wojtas, L.; Eddaoudi, M.; Zaworotko, M. J. *Nature* **2013**, *495*, 80−84.
(8) Petit, J. R.; Jouzel, J.; Raynaud, D.; Barkov, N. I.; Barnola, J. M.; Basile, I.; Bender, M.; Chappellaz, J.; Davis, M.; Delaygue, G.; Delmotte, M.; Kotlyakov, V. M.; Legrand, M.; Lipenkov, V. Y.; Lorius, C.; Pepin, L.; Ritz, C.; Saltzman, E.; Stievenard, M. *Nature* **1999**, *399*, 429−436.
(9) Liu, X.-H.; Ma, J.-G.; Niu, Z.; Yang, G.-M.; Cheng, P. *Angew. Chem., Int. Ed.* **2014**, *54*, 988−991.
(10) Qiu, S.; Xue, M.; Zhu, G. *Chem. Soc. Rev.* **2014**, *43*, 6116−6140.
(11) An, J.; Geib, S. J.; Rosi, N. L. *J. Am. Chem. Soc.* **2010**, *132*, 38−39.
(12) Liao, P.-Q.; Chen, H.; Zhou, D.-D.; Liu, S.-Y.; He, C.-T.; Rui, Z.; Ji, H.; Zhang, J.-P.; Chen, X.-M. *Energy Environ. Sci.* **2015**, *38*, 1213−1214.
(13) Cai, J.; Rao, X.; He, Y.; Yu, J.; Wu, C.; Zhou, W.; Yildirim, T.; Chen, B.; Qian, G. *Chem. Commun.* **2014**, *50*, 1552−1554.
(14) Li, X.-J.; Jiang, F.-L.; Wu, M.-Y.; Chen, L.; Qian, J.-J.; Zhou, K.; Yuan, D.-Q.; Hong, M. *Inorg. Chem.* **2014**, *53*, 1032−1038.

DOI: 10.1021/acs.inorgchem.5b00561
Inorg. Chem. 2015, 54, 5512−5518

(15) Xue, D. X.; Cairns, A. J.; Belmabkhout, Y.; Wojtas, L.; Liu, Y. L.; Alkordi, M. H.; Eddaoudi, M. *J. Am. Chem. Soc.* **2013**, *135*, 7660−7667.
(16) Gong, Y.; Huang, Y.; Jiang, L.; Lu, T. *Inorg. Chem.* **2014**, *53*, 9457−9459.
(17) Sen, S.; Neogi, S.; Aijaz, A.; Xu, Q.; Bharadwaj, P. K. *Inorg. Chem.* **2014**, *53*, 7591−7598.
(18) Sikdar, N.; Hazra, A.; Maji, T. K. *Inorg. Chem.* **2014**, *53*, 5993−6002.
(19) Lee, J. Y.; Olson, D. H.; Pan, L.; Emge, T. J.; Li, J. *Adv. Funct. Mater.* **2007**, *17*, 1255−1262.
(20) Du, L. T.; Lu, Z. Y.; Zheng, K. Y.; Wang, J. Y.; Zheng, X.; Pan, Y.; You, X. Z.; Bai, J. F. *J. Am. Chem. Soc.* **2013**, *135*, 562−565.
(21) Li, B.; Wang, H.; Chen, B. *Chem.—Asian J.* **2014**, *9*, 1474−1498.
(22) Zhao, D.; Timmons, D. J.; Yuan, D.; Zhou, H.-C. *Acc. Chem. Res.* **2011**, *44*, 123−33.
(23) Zhang, J.-P.; Zhang, Y.-B.; Lin, J.-B.; Chen, X.-M. *Chem. Rev.* **2012**, *112*, 1001−1033.
(24) Chen, D.-M.; Shi, W.; Cheng, P. *Chem. Commun.* **2015**, *51*, 370−372.
(25) Chen, D.-M.; Ma, X.-Z.; Zhang, X.-J.; Xu, N.; Cheng, P. *Inorg. Chem.* **2015**, *54*, 2976−2982.
(26) Sheldrick, G. M. *Acta Crystallogr.* **2008**, *A64*, 112−122.
(27) *PLATON* program: Spek, A. L. *Acta Crystallogr., Sect. A* **1990**, *46*, 194−201.
(28) Han, L.; Xu, L.-P.; Qin, L.; Zhao, W.-N.; Yan, X.-Z.; Yu, L. *Cryst. Growth Des.* **2013**, *13*, 4260−4267.
(29) Sarkisov, L.; Harrison, A. *Mol. Simul.* **2011**, *37*, 1248−1257.
(30) Spek, A. *J. Appl. Crystallogr.* **2003**, *36*, 7−13.
(31) Zhang, J.-P.; Liao, P.-Q.; Zhou, H.-L.; Lin, R.-B.; Chen, X.-M. *Chem. Soc. Rev.* **2014**, *43*, 5789−5814.
(32) Chen, B.; Ma, S.; Zapata, F.; Lobkovsky, E. B.; Yang, J. *Inorg. Chem.* **2006**, *45*, 5718−5720.
(33) Wang, J.-H.; Li, M.; Li, D. *Chem. Sci.* **2013**, *4*, 1793−1801.
(34) Li, J.-R.; Ma, Y.; McCarthy, M. C.; Sculley, J.; Yu, J.; Jeong, H.-K.; Balbuena, P. B.; Zhou, H.-C. *Coord. Chem. Rev.* **2011**, *255*, 1791−1823.
(35) Mulfort, K. L.; Farha, O. K.; Malliakas, C. D.; Kanatzidis, M. G.; Hupp, J. T. *Chem.—Eur. J.* **2010**, *16*, 276−281.
(36) Park, H. J.; Suh, M. P. *Chem. Commun.* **2010**, *46*, 610−612.
(37) Hye, J. C.; Dincă, M.; Long, J. R. *J. Am. Chem. Soc.* **2008**, *130*, 7848−7850.
(38) Zhao, X.; Xiao, B.; Fletcher, A. J.; Thomas, K. M.; Bradshaw, D.; Rosseinsky, M. J. *Science* **2004**, *306*, 1012−1015.
(39) Culp, J. T.; Smith, M. R.; Bittner, E.; Bockrath, B. *J. Am. Chem. Soc.* **2008**, *130*, 12427−12434.
(40) Ju, P.; Jiang, L.; Lu, T.-B. *Chem. Commun.* **2013**, *49*, 1820−1822.
(41) Myers, A. L.; Prausnitz, J. M. *AIChE J.* **1965**, *11*, 121−127.
(42) Li, T.; Chen, D.-L.; Sullivan, J. E.; Kozlowski, M. T.; Johnson, J. K.; Rosi, N. L. *Chem. Sci.* **2013**, *4*, 1746−1755.
(43) Xiong, Y.; Fan, Y.-Z.; Yang, R.; Chen, S.; Pan, M.; Jiang, J.-J.; Su, C.-Y. *Chem. Commun.* **2014**, *50*, 14631−14634.
(44) Zhang, S.-Y.; Zhang, X.; Li, H.; Niu, Z.; Shi, W.; Cheng, P. *Inorg. Chem.* **2015**, *43*, 2310−2314.
(45) Haldar, R.; Reddy, S. K.; Suresh, V. M.; Mohapatra, S.; Balasubramanian, S.; Maji, T. K. *Chem.—Eur. J.* **2014**, *20*, 4347−4356.
(46) Chen, D.-M.; Xu, N.; Qiu, X.-H.; Cheng, P. *Cryst. Growth Des.* **2015**, *51*, 961−965.

DOI: 10.1021/acs.inorgchem.5b00561
Inorg. Chem. 2015, 54, 5512−5518